Supplementary data

1. Materials and methods

1.1. Heartbeat detection task: behavioral performance analysis

Behavioral performance, indexed by interoceptive accuracy, was analyzed for each subject by means of signal detection theory (SDT) (Richter and Zimmer, 2018). On the assumption that almost all decisions are subject to uncertainty (Velden, 1982), SDT can be applied whenever two different categories (noise and signal) need to be distinguished. In the heartbeat detection (HBD) model, heartbeats represent the signal and the absence of heartbeats is noise. According to Velden (Velden, 1982), the HBD task can be classified as a yes/no task, whereby a push of a button is to be treated as a 'yes' and its absence as a 'no'. To classify the participants' motor responses, every motor response is assessed for proximity relative to the R-wave of its preceding heartbeat. If the motor response falls within a given time window, this response is considered a *hit*. In the interoceptive condition (IC), to control for heart rate (HR) differences between participants, we time-locked each tapped response with the corresponding time window for each EKG R-peak of the participant's real heartbeat, considering three time windows: 750 ms after the beat for a HR less than 69.76; 600 ms after the beat for a HR between 69.75 and 94.25; and 400 ms after the beat for a HR higher than 94.25 (Salamone *et al.*, 2018). In SDT terminology, the absence of a response during the time window is defined as a *miss*. *False alarm* refers to a response outside the time window, while *correct rejection* means the absence of a response outside the time window. A discrimination index *d*', which is able to separate interoceptive accuracy (*d*') from individual response tendency by reference to these four response categories, was calculated according to the following formula (Macmillan, 2005; Swets, 1986; Velden, 1982):

$$d' = z\left(\frac{\sum hit}{\sum hit + \sum miss}\right) - z\left(\frac{\sum false\ alarm}{\sum false\ alarm + \sum correct\ rejection}\right)$$

The smaller the value of *d*', the worse the discrimination performance and thus the interoceptive accuracy. Z (*p*) is the inverse normal probability corresponding to cumulative probability. For a detailed explanation of the evaluation of HBD task data using SDT, see (Richter and Zimmer, 2018; Thomson and Kristan, 2005). In the exteroceptive condition (EC), the window used was between 0 to 750 ms of the recorded heartbeat.

1.2.1. Image acquisition

MRI acquisition and preprocessing steps are reported in line with the practical guide from the Organization for Human Brain Mapping (Nichols *et al.*, 2017; Poldrack *et al.*, 2017). For anatomical analysis, we obtained whole-brain T1-weighted anatomical 3D scans, spin echo volumes, parallel to the plane connecting the anterior and posterior commissures, with the following parameters: repetition time (TR) = 7489 ms; echo time (TE) = 3420 ms; flip angle = 8º; 196 slices, matrix dimension = 256 x 240; voxel size = 1 x 1 x 1 mm3; sequence duration = 7 minutes.

Functional connectivity analyses were based on resting-state GRE-EPI volumes. Slices parallel to the anterior-posterior commissures, covering the whole brain, were sequential ascending acquired with the following parameters: TR = 2777 ms; TE = 50 ms; flip angle = 90º; 33 slices, matrix dimension = 64 x 64; voxel size in plane = 3.6 mm x 3.6 mm; slice thickness = 4 mm; sequence duration = 10 minutes; number of volumes = 209. Participants were asked to keep eyes closed, to avoid moving or falling asleep, and to think about their routine since waking until the end of the day (Barttfeld et al., 2012; Sedeno et al., 2014).

1.2.2. Image preprocessing and analysis

For VBM analysis, data were preprocessed on the DARTEL Toolbox following validated procedures (Ashburner and Friston, 2000; Couto *et al.*, 2013) on Statistical Parametric Mapping software (SPM12, http://www.fil.ion.ucl.ac.uk/spm/software/spm12/). T1-weighted images in native space were first segmented using the default parameters of the SPM12 (bias regularisation was set to 0.001 and bias FWHM was set to 60-mm cut-off) into white matter

(WM), grey matter (GM), and CFS (these three tissues were used to estimate the total intracranial volume, TIV). Then, we ran the 'DARTEL (create template) module' using the GM and WM segmented images (with the default parameters indicated by the SPM12) to create a template that is generated from the complete data set –and thus increase the accuracy of inter-subject alignment (Ashburner, 2007). Next, we used the 'Normalise to MNI Space module' from DARTEL Tools to affine register the last template from the previous step into the MNI space. This transformation was then applied to all the individual GM segmented scans to also be brought into standard space. Subsequently, all images were modulated to correct volume changes by Jacobian determinants, and avoid a bias in the intensity of an area due to its expansion during warping. Finally, an isotropic Gaussian kernel of 8-mm full width at half maximum was applied to all images. The size of the kernel was selected based on previous recommendations (Good *et al.*, 2001).

Resting-state fMRI scans were preprocessed using the Data Processing Assistant for Resting-State fMRI (DPARSF V2.3) (Chao-Gan and Yu-Feng, 2010), an open-access toolbox that generates automatic analysis pipelines for imaging data. For each preprocessing step, DPARFS called the Statistical Parametric Mapping (SPM) and Resting-State fMRI Data Analysis Toolkit (REST V.1.7) to process the data. Before preprocessing, the first five volumes of each subject's resting-state session were discarded to ensure that magnetization achieved a steady state. Then, images were slice-time corrected (using as reference the middle slice of each volume) and aligned to the first scan of the session to correct head movement (SPM functions). To reduce the effect of motion and physiological artifacts (as cardiac and respiration effects), six motion parameters, CFS and WM signals were removed as nuisance variables (REST default functions). CFS and WM masks for this procedure were derived from the tissue segmentation of each subject's T1 scan in native space with the SPM12 software (after the co-registration of each subject's structural image with the fMRI one). Next, functional images were normalized to the MNI space using the echo-planar imaging (EPI) template from SPM (Ashburner and Friston, 1999), and then they were smoothed using an 8-mm full-width-at-half-maximum isotropic Gaussian kernel (SPM functions). Finally, data was bandpass filtered between 0.01-

0.08 Hz given the relevance of slow frequency in the analysis of resting-state networks (Fox *et al.*, 2005; Raichle, 2009) (REST functions). The participants included had no movements greater than 3 mm and/or rotations higher than 3º. No between group differences were found in the mean (m) rotational (controls: *m* = 0.80, *SD* = 1.6; F-MS: *m* = 0.68, *SD* = 0.68; nF-MS: *m* = 0.44, *SD* = 0.14. One-way ANOVA test: *p*= .70, F = 0,34, R^2 = 0.01) and mean translational parameters (controls: *m* = 1.01, *SD* = 2.3; F-MS: *m* = 0.62, *SD* = 0.42; nF-MS: *m* = 0.63, *SD* = 0.34. One-way ANOVA test: *p* = .69, F = 0.36*)*.

1.2.3. Multivariate analysis: supervised learning models

For classification purposes, three SVM based on interoception markers (interoceptive score, correlation coefficient of GM volume and fatigue, and FC score between L-ACC and R-Ins) were trained and tested in order to differentiate between the two supplied classes (either control and F-MS, F-MS and nF-MS, or control and nF-MS). Taking into account the sample size, 200 iterations of five-fold cross-validation were performed to exploit all data and improve stability (Braga-Neto and Dougherty, 2004). In addition, each feature's relevance was calculated in each iteration by implementing the permutation importance method (Breiman, 2001), which randomly permutes every value in a feature while keeping all remaining features intact, comparing the model's performance with and without the permutation, and establishing their relative weights (or contribution to the classification). Finally, statistical measures (accuracy, sensibility and sensitivity; Supplementary Table e-4) in addition to ROC (Receiver Operating Characteristic) curves (Figure 1.g.) and feature relevance (Figure 1.h.) were averaged and obtained for each model.

2. Supplementary tables

2.1 Supplementary table 1: Demographic and clinical information for behavioral results.

	F-MS	nF-MS	Controls	χ2	p-value
Sex (n)	F=14 / M=1	F=7 / M=5	F=16 / M=6	4.5	.1
				F	
Age (years)	40.87 (10.63)	36.58 (9.96)	35.23 (10.91)	1.29	.28
Education (years)	17.33 (3.75)	15.33 (3.2)	17.55 (2.46)	2.17	.12
EDSS	1.3 (1.95)	1.04 (1.35)			.7
MSSS	1.78 (2.75)	1.31 (1.96)			.62
Years since diagnosis	10.87 (9.45)	8.25 (4.9)			.39
Fatigue	53 (37-56)*	22 (8-32)*	7.5 (0-35)*	-	-

Pearson's chi-square (χ2) test was used to assess sex statistics. Age and education were assessed using One-way ANOVA test**.** To compare EDSS (Kurtzke, 1983), MSSS –(severity assessed by the relationship between EDSS and disease duration (Roxburgh *et al.*, 2005)–, and years of disease evolution between F-MS and nF-MS patients, we used unpaired *t*-tests. Values indicate mean and standard deviation of the mean (in brackets), except for * that indicate minimum and maximum respectively. F: female, M: male. EDSS: Expanded Disability Status Scale. MSSS: Multiple Sclerosis Severity Score.

2.2 Supplementary table 2: VBM results

a. Grey matter atrophy areas of F-MS compared to controls.

	Peaks		**MNI coordinates**			
Number of voxels	***t*-value**	***p*-value**	**X**	**y**	**z**	**Brain area (AAL)**
470	9.21	< .001	-12	-31.5	7.5	Thalamus L
	6.87	< .001	-19.5	-33	-1.5	Hippocampus L
481	8.27	< .001	12	-30	6	Thalamus R
1367	5.27	< .001	12	21	3	Caudate R
	4.49	< .001	15	7.5	15	Caudate R
	3.99	< .001	21	7.5	3	Putamen R
1028	4.98	< .001	51	-40.5	0	Temporal Mid R
	4.40	< .001	48	-36	10.5	Temporal Sup R
	4.11	< .001	46.5	-45	13.5	Temporal Sup R
1031	4.89	< .001	22.5	-9	-18	Hippocampus R
	4.11	< .001	28.5	6	-24	Temporal Pole Sup R
	3.50	< .001	34.5	18	-25.5	Temporal Pole Sup R
1122	4.73	< .001	-12	12	10.5	Caudate L
	4.67	< .001	-13.5	18	-4.5	Caudate L
441	4.71	< .001	-7.5	-12	46.5	Cingulum Mid L
	4.07	< .001	-9	1.5	42	Cingulum Mid L
719	4.68	< .001	-48	-39	21	Temporal Sup L
	4.18	< .001	-58.5	-42	-1.5	Temporal Mid L
95	4.65	< .001	-19.5	-40.5	-45	Cerebelum L
750	4.55	< .001	-36	10.5	-27	Temporal Pole Sup L

	4.47	< .001	-19.5	-9	-16.5	Hippocampus L
702	4.55	< .001	-37.5	-18	7.5	Heschl L
	4.04	< .001	-36	-10.5	15	Insula L
	4.03	< .001	-40.5	-13.5	-6	Temporal Sup L
1234	4.44	< .001	57	-12	-10.5	Temporal Sup R
	4.22	< .001	37.5	-18	15	Insula R
502	4.42	< .001	9	-72	22.5	Cuneus R
206	4.35	< .001	-21	48	-10.5	Frontal Sup Orb L
	4.05	< .001	-31.5	43.5	-10.5	Frontal Mid Orb L
883	4.29	< .001	33	-63	-33	Cerebelum R
	3.83	< .001	25.5	-55.5	-30	Cerebelum R
447	4.23	< .001	24	-33	-22.5	Cerebelum R
429	4.00	< .001	6	43.5	-10.5	Frontal Med Orb R
87	3.96	< .001	-9	-67.5	-36	Cerebelum L
148	3.80	< .001	13.5	42	16.5	Cingulum Ant R
	3.73	< .001	12	27	31.5	Cingulum Mid R
71	3.64	< .001	-25.5	-37.5	-19.5	Fusiform L
69	3.47	< .001	-10.5	-28.5	46.5	Cingulum Mid L

b. Grey matter atrophy areas of nF-MS compared to controls.

	Peaks		**MNI coordinates**			
Number of voxels	***t*-value**	***p*-value**	**X**	**y**	**z**	**Brain area (AAL)**
179	7.44	< .001	-12	-24	9	Thalamus L
700	7.30	< .001	7.5	-16.5	7.5	Thalamus R

	7.14	< .001	7.5	-22.5	1.5	Thalamus R
	5.57	< .001	21	-31.5	-3	Hippocampus R
274	6.68	< .001	-18	-34.5	-1.5	Hippocampus L
1797	4.70	< .001	6	-48	-22.5	Vermis
81	4.26	< .001	-19.5	-40.5	-45	Cerebelum L
182	4.25	< .001	10.5	21	0	Caudate R
	3.34	< .001	21	15	3	Putamen
67	4.25	< .001	25.5	22.5	43.5	Frontal Sup R
187	4.23	< .001	-15	-16.5	-22.5	ParaHippocampal L
	3.80	< .001	-19.5	-10.5	-10.5	Amygdala
95	4.14	< .001	46.5	-9	36	Precentral R
73	3.99	< .001	28.5	-73.5	22.5	Occipital Mid R
280	3.98	< .001	-18	19.5	-3	Putamen L
	3.36	< .001	-15	7.5	-1.5	Pallidum L
216	3.88	< .001	0	-75	4.5	Lingual L
74	3.83	< .001	-25.5	-93	7.5	Occipital Mid L
	3.40	< .001	-36	-88.5	3	Occipital Mid L
91	3.64	< .001	-57	-9	34.5	Postcentral L
95	3.55	< .001	-13.5	-24	42	Cingulum Mid L

c. Grey matter atrophy areas associated to increased levels of fatigue in F-MS/controls.

	Peaks		**MNI coordinates**			
Number of voxels	***t*-value**	***p*-value**	**X**	**y**	**z**	**Brain area (AAL)**

437	7.14	< .001	-15	-31.5	7.5	Thalamus L
	3.41	< .001	-9	-46.5	-3	Lingual L
402	6.68	< .001	10.5	-28.5	4.5	Thalamus R
201	5.29	< .001	-21	-39	-45	Cerebelum R
	3.59	< .001	-10.5	-42	-54	Cerebelum R
549	5.12	< .001	-61.5	-24	-13.5	Temporal Mid L
1302	4.93	< .001	54	-39	0	Temporal Mid R
	4.87	< .001	67.5	-27	-6	Temporal Mid R
	4.82	< .001	61.5	-34.5	-6	Temporal Mid R
265	4.90	< .001	48	-54	31.5	Angular R
3564	4.86	< .001	43.5	-52.5	-25.5	Cerebelum R
	4.65	< .001	28.5	-37.5	-25.5	Cerebelum R
657	4.75	< .001	-7.5	-12	46.5	Cingulum Mid L
	4.23	< .001	-7.5	1.5	42	Cingulum Mid L
	3.59	< .001	-3	-24	51	Paracentral Lobule L
	4.24	< .001	-6	4.5	0	Caudate Head
	3.73	< .001	-12	7.5	10.5	Caudate L
651	4.41	< .001	-40.5	-15	-6	Temporal Sup L
	4.24	< .001	-39	-18	4.5	Heschl L
	3.88	< .001	-43.5	-4.5	-15	Temporal Mid L
242	4.28	< .001	-19.5	48	-12	Frontal Sup Orb L
	4.13	< .001	-31.5	45	-10.5	Frontal Mid Orb L
348	4.27	< .001	9	-72	22.5	Cuneus R
	3.63	< .001	-1.5	-57	22.5	Precuneus L
	3.60	< .001	3	-63	19.5	Cuneus R
195	4.21	< .001	-36	9	-28.5	Temporal Pole Sup L
103	4.18	< .001	36	30	0	Insula R

299	4.16	< .001	-28.5	-39	-21	Fusiform L
464	4.10	< .001	13.5	40.5	18	Cingulum Ant R
	4.08	< .001	13.5	48	6	Frontal Sup Medial R
	3.95	< .001	3	46.5	15	Cingulum Ant R
220	4.06	< .001	-48	-39	19.5	Temporal Sup L
	3.47	< .001	-54	-34.5	12	Temporal Sup L
621	4.00	< .001	37.5	-19.5	4.5	Insula R
	3.93	< .001	39	-18	15	Rolandic Oper R
124	3.93	< .001	-19.5	-57	-30	Cerebelum L
890	3.92	< .001	3	43.5	-7.5	Frontal Mid Orb R
	3.88	< .001	-9	36	-7.5	Cingulum Ant L
	3.75	< .001	7.5	36	-4.5	Cingulum Ant R
72	3.92	< .001	9	3	51	Supp Motor Area R
145	3.85	< .001	-1.5	46.5	30	Frontal Sup Medial L
116	3.72	< .001	10.5	28.5	31.5	Cingulum Mid R
	3.61	< .001	1.5	36	27	Cingulum Ant L
88	3.71	< .001	-24	40.5	36	Frontal Sup L
105	3.71	< .001	21	-7.5	-15	Hippocampus R
82	3.71	< .001	-18	-9	-15	Hippocampus L
95	3.70	< .001	25.5	-66	-48	Cerebelum R
84	3.61	< .001	25.5	24	-24	Frontal Inf Orb R
	3.49	< .001	33	18	-25.5	Temporal Pole Sup R
	3.42	< .001	18	18	-21	Frontal Sup Orb R
52	3.58	< .001	3	43.5	39	Frontal Sup Medial R
	3.42	< .001	4.5	34.5	46.5	Frontal Sup Medial R
51	3.57	< .001	4.5	24	49.5	Frontal Sup Medial R

2.3 Supplementary table 3: Functional connectivity of key interoceptive areas.

Controls	**Ins L**	**Ins R**	**ACC L**	**ACC R**	**SSC L**
Ins R	**0.62** (0.34)	- -	- -	- -	- -
ACC L	**0.18** (0.18)	**0.10** (0.20)	- -	- -	- -
ACC R	**0.10** (0.17)	**0.11** (0.18)	**1.28** (0.18)	- -	- -
SSC L	**0.25** (0.24)	**-0.05** (0.33)	**0.18** (0.15)	**0.16** (0.18)	- -
SSC R	**-0.01** (0.31)	**0.21** (0.21)	**0.11** (0.18)	**0.12** (0.20)	**0.75** (0.45)
F-MS					
Ins R	**0.5292** (0.39)	- -	- -	- -	- -
ACC L	**0.27** (0.1115)	**0.20** (0.2409)	- -	- -	- -
ACC R	***0.27** (0.16)	**0.24** (0.31)	**1.33** (0.31)	- -	- -
SSC L	**0.31** (0.25)	**0.02** (0.37)	**0.10** (0.26)	**0.08** (0.28)	- -
SSC R	**0.03** (0.32)	**0.28** (0.28)	**0.10** (0.26)	**0.09** (0.25)	**0.7656** (0.53)
nF-MS					
Ins R	**0.51** (0.51)	- -	- -	- -	- -

ACC L	**0.24**	**0.19**	-	-	-
	(0.28)	(0.30)	-	-	-
ACC R	**0.14**	**0.17**	**1.32**	-	-
	(0.31)	(0.35)	(0.32)	-	-
SSC L	**0.29**	**-0.11**	**0.17**	**0.18**	-
	(0.37)	(0.47)	(0.37)	(0.38)	-
SSC R	**-0.10**	**0.24**	**0.04**	**0.10**	**0.59**
	(0.42)	(0.35)	(0.34)	(0.33)	(0.48)

Values indicate mean and standard deviation of the mean (in brackets). ***** Increased connectivity between right ACC and left insula in F-MS patients compared to controls (p = .002, t = -3.1, pFDR = 0.04). No difference in connectivity was found between controls and nF-MS patients.

2.4 Supplementary table 4: Statistical measures of supervised models

	control vs F-MS	**F-MS vs nF-MS**	**control vs nF-MS**
Accuracy	0.786 (0.146)	0.656 (0.194)	0.613 (0.18)
Sensitivity	0.65 (0.293)	0.793 (0.264)	0.172 (0.297)
Specificity	0.9 (0.151)	0.542 (0.347)	0.906 (0.154)

Values indicate mean and standard deviation of the mean (in brackets).

3. Supplementary figures

3.1 Supplementary Figure 1: Interoception and Fatigue association

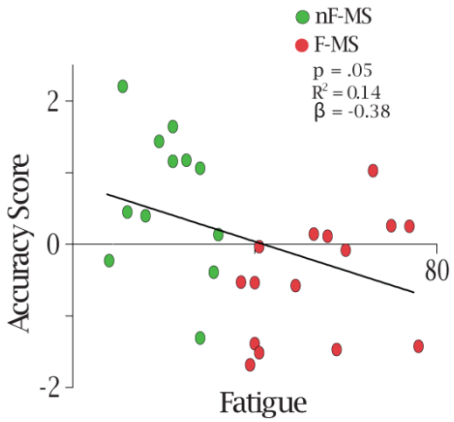

Regression analysis showing a negative association between accuracy score and fatigue when considering F-MS and nF-MS groups.

3.2 Supplementary Figure 2: Gray Matter atrophy

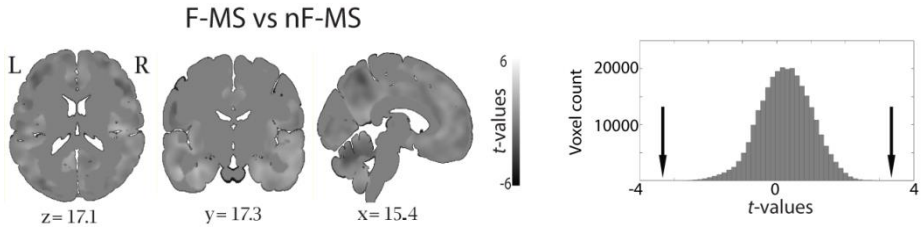

Brain diagrams display the *t*-values maps of gray matter atrophy comparisons between F-MS and nF-MS. Histograms show the number of voxels corresponding to each *t*-value. The arrow points to the *t*-value threshold for results to be considered significant (t = +/- 3.43). As can be appreciated, no significant results were obtained with an alpha level of $p < 0.001$ at the uncorrected voxel level (extent threshold = 50 voxels).

3.3 Supplementary Figure 3: Fatigue and Gray Matter association

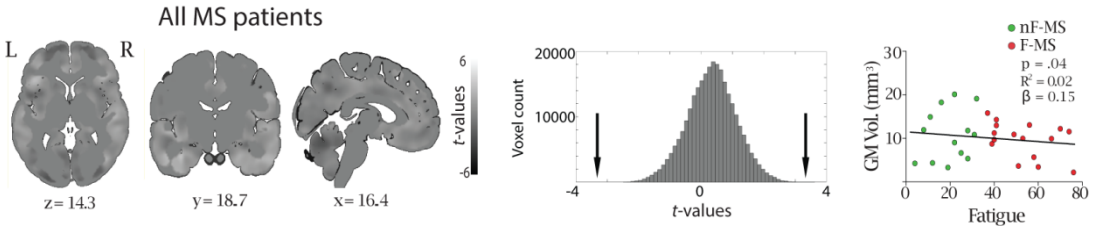

Left: Brain diagrams display the *t*-values maps of the association between gray matter atrophy and Fatigue considering F-MS and nF-MS. Center: Histograms show the number of voxels corresponding to each *t*-value. The arrow points to the *t*-value threshold for results to be considered significant (t = +/- 3.43). As can be appreciated, no significant results were obtained with an alpha level of $p < 0.001$ at the uncorrected voxel level (extent threshold = 50 voxels). Right: scatter plot showing no association between grey matter volume of the areas of significant differences between controls and F-MS patients (y-axes) and fatigue (x-axes), for nF-MS and F-MS.

4. References

Ashburner, J., Friston, K.J., 1999. Nonlinear spatial normalization using basis functions. Hum Brain Mapp. 7**,** 254-66.

Ashburner, J., Friston, K.J., 2000. Voxel-based morphometry--the methods. Neuroimage. 11**,** 805-21.

Ashburner, J., 2007. A fast diffeomorphic image registration algorithm. Neuroimage. 38**,** 95-113.

Braga-Neto, U.M., Dougherty, E.R., 2004. Is cross-validation valid for small-sample microarray classification? Bioinformatics. 20**,** 374-80.

Breiman, L., 2001. Random forests, Vol.

Couto, B., Manes, F., Montanes, P., Matallana, D., Reyes, P., Velasquez, M*., et al.*, 2013. Structural neuroimaging of social cognition in progressive non-fluent aphasia and behavioral variant of frontotemporal dementia. Front Hum Neurosci. 7**,** 467.

Chao-Gan, Y., Yu-Feng, Z., 2010. DPARSF: A MATLAB Toolbox for "Pipeline" Data Analysis of Resting-State fMRI. Front Syst Neurosci. 4**,** 13.

Fox, M.D., Snyder, A.Z., Vincent, J.L., Corbetta, M., Van Essen, D.C., Raichle, M.E., 2005. The human brain is intrinsically organized into dynamic, anticorrelated functional networks. Proc Natl Acad Sci U S A. 102**,** 9673-8.

Good, C.D., Johnsrude, I.S., Ashburner, J., Henson, R.N., Friston, K.J., Frackowiak, R.S., 2001. A voxel-based morphometric study of ageing in 465 normal adult human brains. Neuroimage. 14**,** 21-36.

Kurtzke, J.F., 1983. Rating neurologic impairment in multiple sclerosis: an expanded disability status scale (EDSS). Neurology. 33**,** 1444-52.

Macmillan, N., Creelman, C., 2005. Detection Theory. New York: Psychology Press, https://doi.org/10.4324/9781410611147.

Nichols, T.E., Das, S., Eickhoff, S.B., Evans, A.C., Glatard, T., Hanke, M*., et al.*, 2017. Best practices in data analysis and sharing in neuroimaging using MRI. Nat Neurosci. 20**,** 299-303.

Poldrack, R.A., Baker, C.I., Durnez, J., Gorgolewski, K.J., Matthews, P.M., Munafo, M.R*., et al.*, 2017. Scanning the horizon: towards transparent and reproducible neuroimaging research. Nat Rev Neurosci. 18**,** 115-126.

Raichle, M.E., 2009. A paradigm shift in functional brain imaging. J Neurosci. 29**,** 12729-34.

Richter, F., Zimmer, H., 2018. Analysis of Heartbeat Tracking Tasks by Means of the Signal-Detection Theory. Diagnostica, 64(2), 97–108. . Diagnostica. 64(2), 97–108. .

Roxburgh, R.H., Seaman, S.R., Masterman, T., Hensiek, A.E., Sawcer, S.J., Vukusic, S*., et al.*, 2005. Multiple Sclerosis Severity Score: using disability and disease duration to rate disease severity. Neurology. 64**,** 1144-51.

Salamone, P.C., Esteves, S., Sinay, V.J., Garcia-Cordero, I., Abrevaya, S., Couto, B*., et al.*, 2018. Altered neural signatures of interoception in multiple sclerosis. Hum Brain Mapp. 39**,** 4743-4754.

Swets, J.A., 1986. Form of empirical ROCs in discrimination and diagnostic tasks: implications for theory and measurement of performance. Psychol Bull. 99**,** 181-98.

Thomson, E.E., Kristan, W.B., 2005. Quantifying stimulus discriminability: a comparison of information theory and ideal observer analysis. Neural Comput. 17**,** 741-78.

Velden, M., 1982. Die Signalentdeckungstheorie in der Psychologie. . (Kohlhammer, Ed.) (1. Auflage). Stuttgart.